ELSEVIER

Thermochimica Acta 377 (2001) 63–84

thermochimica acta

www.elsevier.com/locate/tca

The application of temperature-modulated DSC to the glass transition region II. Effect of a distribution of relaxation times

J.M. Hutchinson[a,*,1], S. Montserrat[b]

[a]*Department of Engineering, King's College, University of Aberdeen, Aberdeen AB24 3UE, Scotland, UK*
[b]*Departament de Màquines i Motors Tèrmics, ETSEIT, Universitat Politècnica de Catalunya (UPC), 08222 Terrassa, Spain*

Received 23 October 2000; received in revised form 18 March 2001; accepted 20 March 2001

Abstract

An analysis of temperature-modulated differential scanning calorimetry (TMDSC) in the glass transition region is presented. It extends an earlier and simpler model by introducing a distribution of relaxation times, characterised by a Kohlrausch–Williams–Watts (KWW) stretched exponential parameter β, in addition to the usual kinetic parameters of relaxation, namely the Tool–Narayanaswamy–Moynihan (TNM) non-linearity parameter x and the apparent activation energy Δh^*. The present model describes, more realistically than did its predecessor, all the characteristic features of TMDSC in the glass transition region, and it has been used to examine the effects of the important experimental variables, namely the period of modulation and the underlying cooling rate. It is shown that, for typical experimental conditions in practice, it is likely that there well be an interaction between the vitrification process, due to the underlying cooling rate, and the dynamic glass transition whereby the complex heat capacity C_p^* shows a sigmoidal decrease in a temperature range dependent on the modulation frequency. Accordingly, care must be exercised in the quantitative evaluation of TMDSC data in the glass transition region, and suggestions are made regarding the optimum procedures in this respect. Also, by comparing the cooling rate and modulation period required to define the same transition temperature for conventional DSC and C_p^*, respectively, a correspondence between them is obtained which allows the magnitude of temperature fluctuations in Donth's fluctuation dissipation theorem to be evaluated. Finally, it is shown that β and x have similar effects on conventional DSC cooling curves, but have very different effects on C_p^*, whereby there is little effect of x but a significant broadening of the transition as β decreases. It is argued that the breadth of the C_p^* transition therefore provides a measurement of β independent of the value of x, thus resolving a problem that has existed for some years.

Keywords: Temperature-modulated differential scanning calorimetry; Glass transition region; Kinetic models; Fluctuation dissipation theorem

1. Introduction

The technique of temperature-modulated differential scanning calorimetry (TMDSC), which was introduced by Reading and co-workers some 8 years ago or so [1–4], has seen a very rapid growth in use, and is now commercially available in several versions, including Modulated DSC (MDSC) from TA Instruments,

* Corresponding author. Tel.: +44-1224-272791; fax: +44-1224-272497.
E-mail addresses: j.m.hutchinson@eng.abdn.ac.uk (J.M. Hutchinson), montserrat@mmt.upc.es (S. Montserrat).

[1] Work done while on a European Science Exchange Programme (ESEP) visit to UPC, and funded by the Royal Society (UK).

0040-6031/01/$ – see front matter
PII: S0040-6031(01)00542-1

Alternating DSC (ADSC) from Mettler–Toledo, and Dynamic DSC (DDSC) from Perkin-Elmer. The fundamental principle of TMDSC is to superpose a periodically modulated temperature profile on top of the linear temperature ramp with time (which may be either heating or cooling) that is characteristic of conventional differential scanning calorimetry (DSC).

The main differences between each of the various implementations of this principle mentioned above lie in (i) the type of periodic modulation that is utilised, and (ii) the way in which the modulated heat flow signal is analysed. In many ways the most convenient modulation to use is sinusoidal, and this is adopted in both MDSC and ADSC, the two techniques that are most commonly used. On the other hand, there has been considerable discussion about the relative merits of the two principal methods of analysis, namely that of ''reversing'' and ''non-reversing'' heat flows and that of the complex heat capacity [5]. We believe there is greater merit in the latter approach, and consequently we develop the analysis here in terms of the complex heat capacity and its in-phase and out-of-phase components. As an illustration, we have shown for both polycarbonate [6] and an epoxy resin [7] that, contrary to what has been suggested by others [8], the non-reversing heat flow does not in general provide a good measure of the enthalpy loss on ageing a glassy polymer below its glass transition temperature (T_g).

In fact, the analysis of TMDSC in the glass transition region is rather appealing as the glass transition is a kinetic effect, with a response that depends on the thermal history, and the thermal history in TMDSC is both complex and precisely defined. In earlier work [9–11], we used a simple, single relaxation time kinetic model to predict the response of a glassy material to TMDSC in the glass transition region, and we were able to model semi-quantitatively all of the characteristic features of the response that are observed experimentally. These features may be summarised as follows:

1. the ''total'' or ''average'' heat capacity, $C_{p,\mathrm{ave}}$, is essentially the same as that obtained by conventional DSC at the same underlying heating rate;
2. the ''complex'' and ''in-phase'' heat capacities are very similar, and display a sigmoidal change from glassy to liquid-like values at a temperature that is often referred to as a ''dynamic'' glass transition temperature, and that is dependent on the modulation period;
3. the ''out-of-phase'' heat capacity and the phase angle between heat flow and heating rate are very similar in appearance, both displaying a (negative) peak at a temperature essentially equal to the dynamic glass transition temperature.

In addition to these features, it is also common to observe ripples on the experimental TMDSC output traces [6,7,12,13]. These ripples have also been described by this simple model, and are shown to be a consequence of the windowing technique used for the Fourier transformation of the modulated heat flow signal.

Besides describing these important features of the TMDSC response, the simple model also has predictive capabilities, and can be used to determine the effects both of experimental variables, such as frequency and amplitude of temperature modulation, and the underlying heating or cooling rate, and also of material variables, such as the enthalpic state of the sample, or material parameters such as the activation energy or non-linearity parameter [11]. This has been useful in furthering our understanding of, for example, the relationship between the dynamic glass transition temperature and that measured in cooling experiments in conventional DSC, or of the interpretation of the physical meaning of the out-of-phase heat capacity.

Despite these successes of this simple model, it was recognised at the time that is was unrealistic in two principal aspects. First, the model assumed that the sample could follow exactly the prescribed temperature programme, whereas in practice this will not be the case as a result of heat transfer effects; and second, the assumption of only a single relaxation time deliberately overlooked, for reasons of simplicity, the known existence of a distribution of relaxation times which governs the response of the sample.

The first aspect, that of heat transfer, has, in the time since our earliest application of the simple model, been addressed by a number of workers [14–16], most commonly in connection with the accurate measurement of heat capacity. With respect to the application of TMDSC to the glass transition region, the effect of heat transfer on the phase angle has received particular attention [17–19], and has led to a procedure for

correcting the phase angle for heat transfer effects in the T_g region [17,18] which has now been incorporated into the software for ADSC analysis [20]. Neglecting the effects of heat transfer in our present theoretical model for the response of glasses in TMDSC may, therefore, be justified on the basis of there being a satisfactory procedure for correcting experimental data to allow for such effects.

The second aspect, that of a distribution of relaxation times, has recently been treated by several workers [21–25]. As noted above, the single relaxation time model was able to reproduce semi-quantitatively all of the important features of the TMDSC response, but the changes in, for example, the complex heat capacity and the phase angle at the glass transition were much sharper than those observed experimentally [9–11]. This is just one of the quantitative aspects of TMDSC that will be examined here in the light of a more realistic model in which a distribution of relaxation times is incorporated.

2. Theoretical analysis

2.1. Basic model

In our earlier single relaxation time model, we made use of a constitutive equation which had previously been successfully applied to the analysis of the response of glasses in conventional DSC experiments [26], and which described the enthalpy (H) changes with time (t) of a sample subjected to a constant heating or cooling rate (q):

$$\frac{\mathrm{d}\delta}{\mathrm{d}t} = -\Delta C_p\, q - \frac{\delta}{\tau(T,\delta)} \tag{1}$$

where $\delta = H - H_\infty$ is the excess enthalpy relative to its equilibrium value (H_∞) at a given temperature (T), $\Delta C_p = C_{pl} - C_{pg}$ the heat capacity (C_p) increment between its values in the glassy (C_{pg}) and liquid-like (C_{pl}) states, and τ the single relaxation time. The relaxation time is known to be both temperature and structure (here characterised by δ) dependent, and was earlier taken to be described by the following equation:

$$\tau = \tau_r \exp[-\theta(T - T_r)] \exp\left[-(1-x)\frac{\theta\delta}{\Delta C_p}\right] \tag{2}$$

where τ_r is the value of τ in equilibrium at an arbitrary reference temperature T_r, the parameter θ is approximately related to an apparent activation energy Δh^* ($\theta \approx \Delta h / RT_g^2$), and x ($0 \le x \le 1$) is the non-linearity parameter describing the relative contributions of temperature and structure to the relaxation time [27], with smaller values of x implying greater non-linearity.

Eq. (2) is equivalent, within a narrow temperature interval around T_g (which may be taken as T_r), to the (slightly modified) Tool–Narayanaswamy–Moynihan (TNM) [28–30] equation:

$$\tau = \tau_g \exp\left[\frac{x\,\Delta h^*}{RT} + \frac{(1-x)\,\Delta h^*}{RT_f} - \frac{\Delta h^*}{RT_g}\right] \tag{3}$$

where τ_g is the relaxation time in equilibrium at T_g. The structure of the glass is now defined by the fictive temperature T_f, and the last term inside the brackets has been incorporated into the usual TNM equation in order to eliminate the unphysical values of the pre-exponential factor that otherwise result.

2.2. Distribution of relaxation times

We turn now to the way in which a distribution of relaxation times is incorporated into the model. In common with most workers, we make use of a non-exponential response function:

$$\phi(t) = \exp\left[-\left(\frac{t}{\tau}\right)^{\beta}\right] \tag{4}$$

which is formally equivalent to a continuous spectrum of relaxation times whose width is inversely related to the exponent β ($0 \le \beta \le 1$). This response function is associated with the names of Kohlrausch [31] and of Williams and Watts [32], and hence is often referred to as the KWW equation or stretched exponential.

Contrary to the simplistic, and erroneous, application of this response function by numerous authors, in which $\phi(t)$ is associated with a normalised excess enthalpy $[(H(t) - H_\infty)/H_\infty]$ and Eq. (6) is fitted to isothermal enthalpy recovery data with a constant value of τ, the use of this response function is complicated by the need to allow for both a temperature and a structure dependence of the relaxation time (e.g. through Eqs. (2) and (3)) even for the simplest of thermal histories such as a quench from equilibrium

to an isothermal annealing temperature. This problem was overcome by the introduction by Narayanaswamy [29] of the concept of a reduced time, which serves to linearise the response.

The importance of the linearisation introduced by the reduced time is that it allows the response to any thermal history to be derived by the application of the Boltzmann superposition principle. Thus, when the response function is written in terms of the reduced time ζ:

$$\phi(\zeta) = \exp\left[-\left(\frac{\zeta}{\tau_r}\right)^{\beta}\right] \tag{5}$$

where τ_r is a characteristic relaxation time in equilibrium at a reference temperature T_r, any general thermal history, which may be considered to be composed of successive instantaneous T-jumps of magnitude dT followed by isothermal periods of duration dt, such that $q = dT/dt$, will result in an excess enthalpy given by

$$\delta(\zeta) = -\Delta C_p \int_0^{\zeta} \phi(\zeta - \zeta') \frac{dT}{d\zeta'} \, d\zeta' \tag{6}$$

The convolution integral in Eq. (6) is the fundamental constitutive equation of the system, in which a distribution of relaxation times is introduced by means of the stretching exponent β in Eq. (5). It is worth noting that this approach is fundamentally different from that utilised earlier for the single relaxation time model. The single relaxation time model approach does not make use of any response function; instead, the time (or temperature) dependence of the excess enthalpy is obtained directly from Eq. (1), which relates the rate of change of δ to its instantaneous value, and hence does not predict any memory effects. In order to introduce memory effects by this approach, it is necessary to include a distribution of relaxation times, as was done in the KAHR model [27]. On the other hand, the approach immediately above in which the response is obtained from the convolution integral in Eq. (6) necessarily introduces memory effects, in the same way as does the Boltzmann superposition principle in linear viscoelasticity. Furthermore, memory effects will be included even when the stretching exponent β is unity, and the stretched exponential becomes a simple exponential, equivalent to the decay for a single relaxation time.

2.3. Application to TMDSC

The model described above is applied to TMDSC by defining the temperature modulations as

$$T = T_0 + q_{av}t + A_T \sin(\omega t) \tag{7}$$

and hence the heating rate modulations as

$$q = \frac{dT}{dt} = q_{av} + A_T \omega \cos(\omega t) \tag{8}$$

where T_0 is the initial temperature, q_{av} the underlying heating ($q_{av} > 0$) or cooling ($q_{av} < 0$) rate, A_T the amplitude of the temperature modulations, and ω is the modulation frequency, related to the period of modulations $t_p = 2\pi/\omega$.

These temperature and heating rate modulations are superimposed on a standard three-step thermal cycle, which includes the following stages:(i) cooling at constant underlying rate from equilibrium at a temperature above T_g to an annealing temperature T_a in the glassy region; (ii) isothermal annealing at T_a for a time t_a such that the excess enthalpy reduces by an amount $\overline{\delta}$; (iii) reheating from T_a at constant underlying rate until equilibrium is again established above T_g. This complete three-step cycle defines the thermal history from which the time evolution of the excess enthalpy is obtained.

For the implementation of the present model, we make use of the following values for the material constants: $C_{pl} = 1.6, C_{pg} = 1.3$, and $\Delta C_p = 0.3$ in $\mathrm{J\,g^{-1}\,K^{-1}}$, $T_r = 373\,\mathrm{K}, \tau_r = 100\,\mathrm{s}$, $\Delta h^*/R = 80\,\mathrm{kK}$ ($\Delta h^* \approx 665\,\mathrm{kJ\,mol^{-1}}$).

The other material constants (x and β) and the values of the experimental parameters (q_{av}, A_T and ω (or t_p) for the definition of the heating rate modulations, together with the initial temperature T_0 and the annealing temperature and time, T_a and t_a, respectively) are inputs for each solution of the model.

The constitutive equation is evaluated using a stepwise integration procedure using Matlab software, with a time step of 2 s typically. The temperature step will depend upon the underlying rate, but is typically of the order of 0.05–0.1 K. For any given simulation, the final choice of these steps is constrained also by the choice of the period of the modulations, with the requirement that there be at least 12 points within any modulation period.

Relative to an arbitrary value of the enthalpy in equilibrium at the reference temperature T_r, the

enthalpy in equilibrium at any other temperature T is given by

$$H_\infty(T) = -C_{pl}(T_r - T) \tag{9}$$

and the instantaneous enthalpy at any temperature is then given as

$$H(T) = H_\infty(T) + \delta(T) \tag{10}$$

where $\delta(T)$ is found from the evaluation of the constitutive equation. Of course, during the isothermal annealing step (stage (ii) of the three-step thermal cycle) both H and δ will be functions of both temperature and time.

Finally, the heat flow (HF) is evaluated as

$$\mathrm{HF} = \frac{\mathrm{d}H}{\mathrm{d}t} \tag{11}$$

by a stepwise differentiation of the enthalpy. The heat flow modulations obtained in this way show quite clearly the typical features of TMDSC in the glass transition region, namely a change in the average heat flow between the glassy and equilibrium liquid-like states, and a change in the amplitude of the modulations. In addition, some more complicated features also appear, dependent upon the specific conditions (for example, the amount of annealing at T_a) of the experiment. The quantitative analysis of these modulations therefore requires a Fourier transformation of the data, as described immediately below.

2.4. Fourier transformation

A sliding Fourier transformation is made, using the 'fft' routine in the Matlab software, of a single cycle of the heating rate and of the corresponding data for the heat flow modulations. The sliding transform is made point by point over the whole time span corresponding to the temperature change from T_0 to T_a during cooling (stage (i) of the three-step thermal cycle) and that from T_a to T_0 during heating (stage (iii) of the three-step thermal cycle).

During the isothermal annealing process at T_a (stage (ii) of the three-step thermal cycle), the temperature modulations are not imposed continuously throughout the duration of the annealing time t_a, since this can typically be very long and would involve an excessive amount of computation. Instead, the annealing process is allowed to proceed with equal intervals of logarithmic time, usually 10 steps per decade, with short bursts of four cycles of modulations at each of these steps. A sliding Fourier transformation of single cycles of the heating rate and of the corresponding heat flow data is made in the same way as described immediately above for the cooling and heating stages. Four possibilities are available for this isothermal stage: (i) to anneal for a specified time t_a; (ii) to reduce the excess enthalpy by a specified amount $\overline{\delta}$; (iii) to reduce the excess enthalpy to a specified value δ; and (iv) to anneal to equilibrium ($\delta = 0$) at that temperature T_a.

This Fourier transformation procedure gives the following quantities $\langle q \rangle$ is the average value of the heating rate ($=q_{av}$), $\langle \mathrm{HF} \rangle$ the average value of heat flow, A_q the amplitude of the heating rate ($=A_T\omega$), A_{HF} the amplitude of heat flow, ϕ the phase angle between heating rate and heat flow.

From these transformed quantities it is possible to evaluate a number of different heat capacities. As explained in Section 1, we adopt the complex heat capacity approach originally proposed by Schawe [5], and use this to define an "average" ($\langle C_p \rangle$ or $C_{p,\mathrm{ave}}$) and a complex (C_p^*) heat capacity, the latter being separated into in-phase (C_p') and out-of-phase (C_p'') components, as follows:

$$\langle C_p \rangle = C_{p,\mathrm{ave}} = \frac{\langle \mathrm{HF} \rangle}{\langle q \rangle} \tag{12}$$

$$C_p^* = \frac{A_{\mathrm{HF}}}{A_q} \tag{13}$$

$$C_p' = C_p^* \cos\phi \tag{14}$$

$$C_p'' = C_p^* \sin\phi \tag{15}$$

It transpires that the phase angle ϕ is nearly always rather small (typically $|\phi| < 0.1$ rad) in the glass transition interval, and hence C_p' and C_p^* are approximately equal, while $C_p' \approx \phi\ C_p^*$. In most cases, therefore, it suffices to evaluate C_p^* and ϕ.

3. Results and discussion

3.1. Response to three-step cycles

In previous work with the single relaxation time model [11], we showed how it was possible to predict

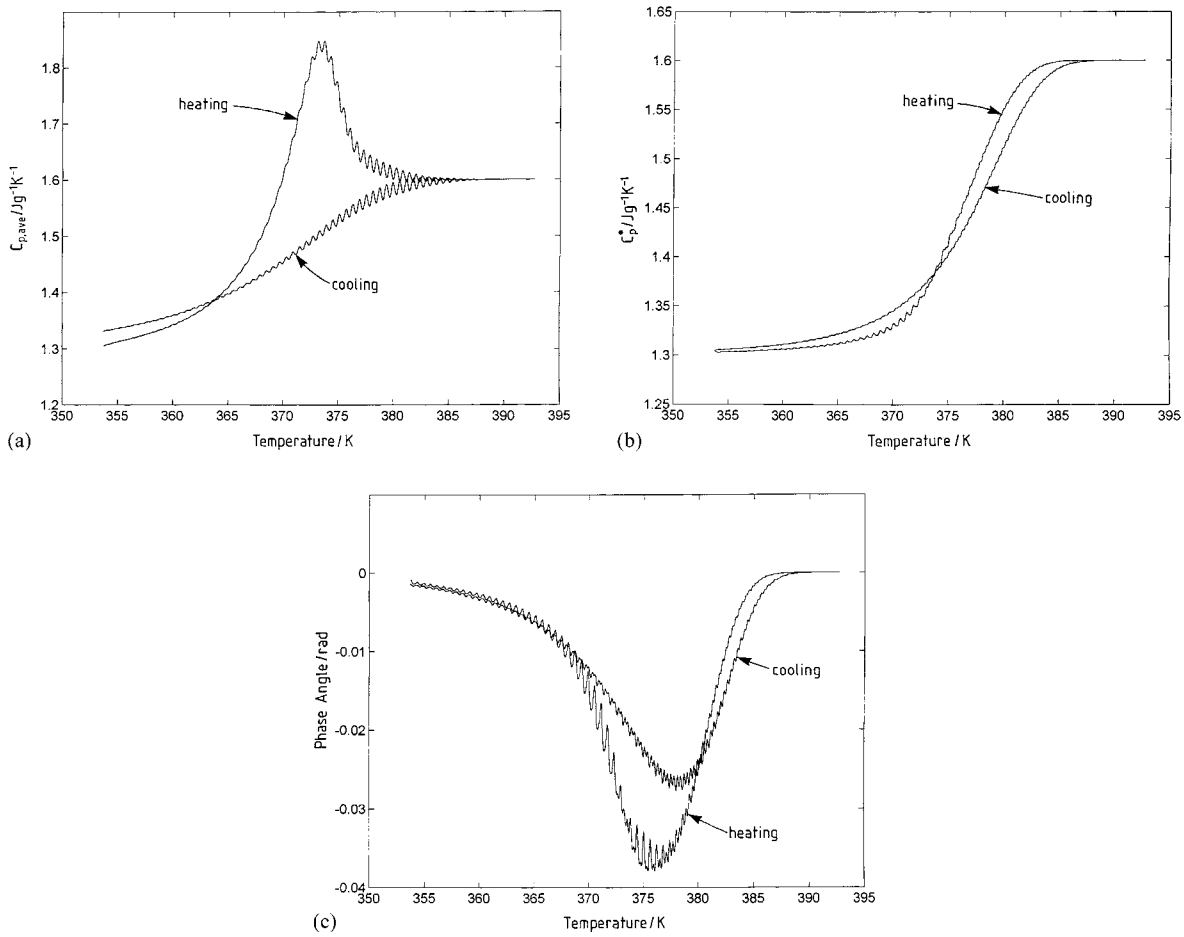

Fig. 1. Average heat capacity (a), complex heat capacity (b), and phase angle (c) during cooling and heating stages (as indicated) of a three-step thermal cycle. Cooling stage: $q_{av} = -1.5$ K min^{-1}, $A_T = 0.5$ K, $t_p = 24$ s. Heating stage: $q_{av} = 0.6$ K min^{-1}, $A_T = 0.5$ K, $t_p = 60$ s. Material parameters: $\beta = 0.4$, $x = 0.4$. Annealing stage at $T_a = 353$ K defined by $\overline{\delta} = 2.015$ J g^{-1}.

the characteristic features of TMDSC in the glass transition region, which were listed in Section 1. Our starting point for discussing the predictions of the model with a distribution of relaxation times is to show that the same features are recovered here also. Fig. 1a–c show, respectively, the average heat capacity, complex heat capacity and the phase angle for the cooling and heating stages of a three-step cycle in which the sample, initially in equilibrium ($\delta = 0$) at temperature $T_0 = T_r + 20$ K (=393 K), was cooled at an underlying rate of 1.5 K min^{-1} down to the annealing temperature $T_a = T_r - 20$ K (=353 K), annealed for a time t_a such that the excess enthalpy reduced by an amount $\overline{\delta} = 2.015$ J g^{-1} before being reheated at an underlying rate of 0.6 K min^{-1} back to the temperature T_0. During the cooling stage, the modulation period was 24 s, whereas it was 60 s during the heating stage, both with a temperature amplitude of 0.5 K. The non-exponentiality and non-linearity of the response of the sample were characterised, respectively, by $\beta = 0.4$ and $x = 0.4$. We can identify from these curves a number of characteristic features, as for the single relaxation time model.

The average heat capacity shows a sigmoidal change from liquid to glass on cooling, whereas on heating there is the characteristic endothermic peak. In fact, on cooling it is evident that the asymptotic glassy state is never achieved, since the heat capacity is

always greater than the glassy value of 1.3 J g^{-1} K^{-1}; this is a direct consequence of the broadening of the transition interval by the introduction of the stretching exponent $\beta = 0.4$. Likewise, for the same reason, the endothermic peak on heating is broader than its counterpart for the single relaxation time model (Fig. 1a in [11]) even though the sample in the present work has been substantially annealed ($\overline{\delta} = 2.015$ J g^{-1}) before reheating.

Ripples are also evident on both the cooling and heating curves, occurring most markedly on the high temperature side of the relaxation in both cases, though slightly smaller in amplitude than the ripples observed from the response of the single relaxation time model [11]. By considering, for example, the temperature interval between 375 and 385 K, it is a simple matter to verify that these ripples have a frequency equal to that of the imposed temperature modulations for both cooling and heating, as has been observed experimentally [6].

Apart from the ripples, these curves for the average heat capacity are, of course, essentially the same as those that would be obtained by conventional DSC at the same underlying cooling and heating rates, and for the same amount of annealing at T_a. In fact, the difference in area between the heating and cooling curves in Fig. 1a is 2.035 J g^{-1}, which is almost identical to the input value of $\overline{\delta} = 2.015$ J g^{-1}. The small difference is due to the truncation error at low temperature which is exacerbated by the cooling curve's not reaching an asymptotic glassy state; the Fourier transformed curves do not end exactly at 353 K on cooling or begin at 353 K on heating, but half a cycle from this temperature in each case, and the effect is, therefore, to overestimate $\overline{\delta}$ from the area difference since the cooling curve lies above the heating curve.

Turning now to the complex heat capacity, it can be seen that this displays a sigmoidal change both on cooling and on heating, a feature that is well known from experimental observations. Again, as for the average heat capacity, the change is less abrupt than for the earlier single relaxation time model [11], even though the initial glassy state prior to heating has a lower excess enthalpy in the present case, and this is a direct result of the inclusion of a distribution of relaxation times. The crossing over of the two curves can be attributed to the combination of two effects: first, the shorter period (24 s) for the cooling curve means that the mid-point of the sigmoid for cooling occurs at higher temperature than it would for the period (60 s) used for the heating curve; and second, the effect of annealing prior to heating is to shift the onset part of the heating sigmoid to higher temperatures while leaving the endset part relatively unaffected [6,11]. Ripples are also evident on both cooling and heating traces, most noticeably in the onset region of the heating trace, a feature that was noted earlier for the single relaxation time model [11] as well as in experimental data for polycarbonate [6] and epoxy resin [7].

The final set of data in Fig. 1 relates to the phase angle. As for the single relaxation time model, a negative peak is apparent, here both on cooling and on heating, but the magnitude of the peak at about 0.04 rad is considerably smaller than that for the single relaxation time model, as well as being correspondingly broader. In fact, comparing the shape of the heating trace with experimental data for polycarbonate [6] we note that the experimental results for well annealed samples, with $t_a \approx 1000$ h, have maximum departures of about 0.08 rad and half-widths of about 2 K, indicative of a much sharper peak than that shown here. The implication is that the value of $\beta = 0.4$ selected here is too small to represent the relaxation spectrum for polycarbonate.

In general, therefore, it is clear that this analysis reproduces the characteristic features of TMDSC in the glass transition region, and that the response is broader than that obtained by the single relaxation time model. This is, in fact, just what would have been anticipated intuitively, and therefore affords a pleasing confirmation of the validity of the present approach. It is interesting now to examine independently the effects of the various parameters, both experimental and material, on the detailed characteristics of the response, and this is reported in the separate sections that follow.

3.2. Effect of period of modulation during heating when $t_p q_{av}$ = constant

The effect of the period of modulation is most clearly seen in the complex heat capacity, such as the family of heating curves shown in Fig. 2. For each curve, the state of the glass prior to heating in the

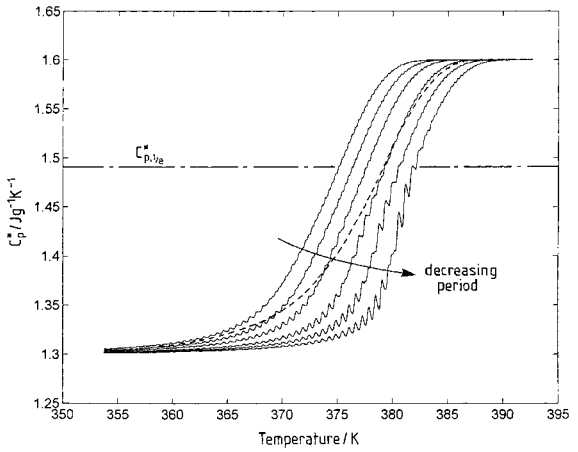

Fig. 2. Complex heat capacity during heating in TMDSC following cooling at $-1.5\ \mathrm{K\ min^{-1}}$ from 393 to 353 K, and annealing at 353 K until $\overline{\delta} = 2.015\ \mathrm{J\ g^{-1}}$. Periods of modulation are 6, 12, 24, 60, 120 and 240 s from right to left, and the underlying heating rate was varied for each curve such that $t_\mathrm{p} q_\mathrm{av} = 0.6$ K. The other parameter values are: $A_T = 0.5$ K, $\beta = 0.4$ and $x = 0.4$. The dashed line shows C_p^* on cooling, with $t_\mathrm{p} = 24$ s, while the dash-dotted line indicates the value of C_p^* which is $\Delta C_p/e$ below $C_{p\mathrm{l}}$.

TMDSC was always the same, namely annealed at $T_\mathrm{a} = 353$ K for sufficient time ($t_\mathrm{a} \approx 78$ h) for the enthalpy to decrease by $2.015\ \mathrm{J\ g^{-1}}$ following cooling at $q_\mathrm{av} = -1.5\ \mathrm{K\ min^{-1}}$, with $A_T = 0.5$ K and $t_\mathrm{p} = 24$ s, from equilibrium at 393 K (the complex heat capacity on cooling is shown by the dashed line in Fig. 2). It can be seen that reducing the period of modulation shifts the curves to higher temperature, and by an amount that should be determined by the activation energy. On closer inspection, though, it is evident that, overlooking in this respect the ripples, the curves will not superpose by means of a horizontal shift. Rather, there is a subtle change in shape in which the curves shift more rapidly in the onset region than they do in the endset region. The onset region is that part that is most influenced by prior annealing [6], as was noted earlier, and the curves in Fig. 2 certainly involve an annealed sample, with $t_\mathrm{a} \approx 78$ h. What is interesting, though, is that the same annealed state is manifest as slightly differently shaped curves when the heating scan involves different periods.

It should be pointed out, however, that it is not only the period of modulation that has been changed for the different curves in Fig. 2. In addition, as the period was changed so also was the underlying heating rate. The reason for this is that it is necessary to include at least, say, ten modulations within the transition interval in order that the Fourier transformation procedure be valid, which implies that the product of t_p and q_av be less than one tenth of the width (in K) of the transition. If we consider the transition to be 10 K wide (it will depend on both β and x), then the requirement is $t_\mathrm{p} q_\mathrm{av} < 1$ K, and we choose here $t_\mathrm{p} q_\mathrm{av} = 0.6$ K. The alternative is to use the slowest underlying heating rate (i.e. that appropriate to the longest period modulations) for all the modulation periods, but this is not convenient in practice as it would involve very long experimental times.

As a consequence of the subtle change of shape, the evaluation of the shifts of the curves in Fig. 2 as the period changes will depend upon the region of the curves that is used. For example, if the curves are shifted at their mid-points, which define temperatures $T_\mathrm{mid}(\omega)$, then it can be seen that this already enters the distorted region, at least for the higher frequencies, such that the shift is greater than it should be, and that the activation energy is thereby reduced. This is shown in Fig. 3, where the open circles represent the plot of $\ln(t_\mathrm{p})$ versus $1/T_\mathrm{mid}$; the slope of the line drawn gives a reduced activation energy of $\Delta h^*/R = 73.7$ kK in comparison with the input value of 80 kK, while

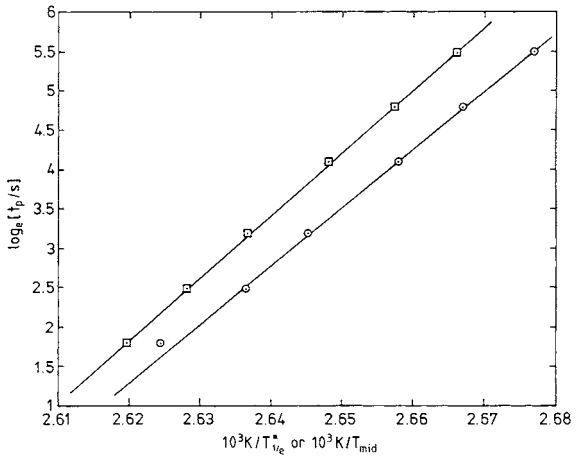

Fig. 3. Plots of $\ln(t_\mathrm{p})$in seconds versus reciprocal temperature for both T_mid (open circles) and $T^*_{1/e}$ (open squares) evaluated from the curves in Fig. 2. The slopes of the lines give the reduced apparent activation energy $\Delta h^*/R$.

there is a marked deviation from this line for the shortest period.

A better location in which to evaluate the shifts may instead be at that value of C_p^* which is a fraction $1/e$ of ΔC_p^* less than C_{pl} and which we denote here by $C_{p,1/e}^*$. The reason for this is not only that it thereby includes a wider range of periods for which this value of C_p^* lies within an undistorted region of the curves, but also because $C_{p,1/e}^*$ has a significance in another context, to be considered further below. In fact, a hint about this significance is provided by a comparison of the curves for $t_p = 24$ s on heating and on cooling, the latter shown by the dashed line in Fig. 2. This comparison shows clearly the shape change of the heating curves due to the annealing, but also shows that the cooling and heating curves intersect at $C_{p,1/e}^*$. This value of complex heat capacity, therefore, appears as one which is independent of the amount of annealing, and also of whether one considers the cooling or heating curves, and hence represents the optimum part of the curve for the purposes of superposition. If we denote by $T_{1/e}^*$ the temperature at which $C_{p,1/e}^*$ occurs, then the plot of $\ln(t_p)$ versus $1/T_{1/e}^*$, shown by open squares in Fig. 3, gives a linear relationship with a slope of $\Delta h^*/R = 79.5$ kK over the whole range of periods, thus recovering almost exactly the input value of the activation energy.

Considering now the average heat capacity, there should theoretically be no effect of the period of the modulations since $C_{p,\mathrm{ave}}$ should be essentially the same as C_p obtained by conventional DSC. However, since the underlying heating rate was modified to suit the period in order to accommodate sufficient modulations in the transition interval, the $C_{p,\mathrm{ave}}$ curves corresponding to the C_p^* curves in Fig. 2 do in fact show a dependence, but on q_{av} and not on t_p. Fig. 4 shows the $C_{p,\mathrm{ave}}$ curves, where the usual shift of the endothermic peak to higher temperatures and greater magnitude of peak height is observed. It is interesting to note that for the slowest heating rates there appear two peaks, or a peak and a shoulder, which is a direct result of the distribution of relaxation times, and which has been discussed before in respect of its appearance in conventional DSC [27,33,34]. Such effects in the glass transition region are more likely to appear when the heating rate is slower than the previous cooling rate, which tends to be the condition under which many TMDSC experiments are run.

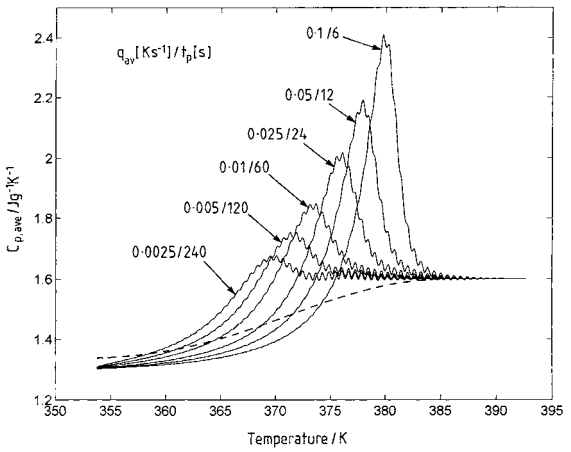

Fig. 4. Family of $C_{p,\mathrm{ave}}$ curves for heating in TMDSC with the rates (in K s^{-1}) and period (in seconds) shown against each curve. Previous history was cooling, indicated by dashed line (which has been smoothed), at -1.5 K min^{-1} and annealing at 353 K until $\overline{\delta} = 2.015$ J g^{-1}. Other parameters: $A_T = 0.5$ K, $\beta = 0.4$, $x = 0.4$.

The effect of the modulation period on the phase angle is shown in Fig. 5. It can be seen that the main effect is to shift the negative peak in the phase angle to higher temperatures as the period decreases. In addition, though, the peaks become sharper (as measured, for example by peak width at half height) and with an increasingly large maximum departure from zero as

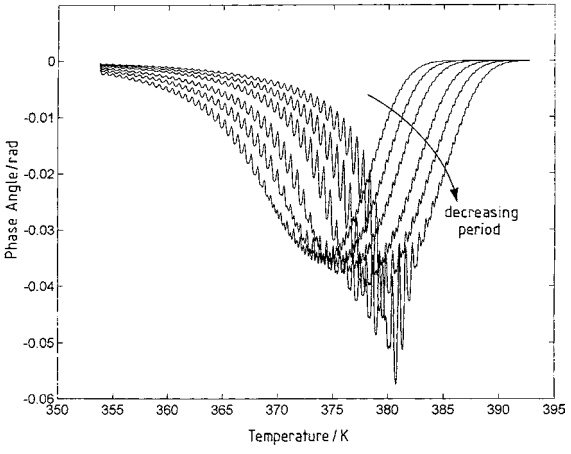

Fig. 5. Family of phase angle curves for heating in TMDSC with modulation periods of 6, 12, 24, 60, 120 and 240 s, and the underlying heating rate varied such that $t_p q_{\mathrm{av}} = 0.6$ K. Previous history and other parameter values are the same as for Fig. 2.

the frequency increases. This corresponds to the distortion of the C_p^* curves, shown in Fig. 2, in the onset region, and means that the activation energy calculated from, for example, the temperatures at which the negative peaks in phase angle occur as a function of the period of modulation, will be slightly small than the correct value for the same reason as was discussed above in respect of Fig. 3.

3.3. Effect of period of modulation during cooling when q_{av} = constant

On cooling at a given rate q_{av}, the average heat capacity displays a sigmoidal change from $C_{p\mathrm{l}}$ to $C_{p\mathrm{g}}$ from which a glass transition temperature or fictive temperature may be found. Sometimes, for convenience, this is taken as the temperature T_{mid} at which $C_{p,\mathrm{ave}}$ is midway between $C_{p\mathrm{l}}$ and $C_{p\mathrm{g}}$. For the purposes of comparison with a transition temperature derived from the complex heat capacity, however, there would be a certain logic in making use of a temperature $T_{1/e}^{\mathrm{av}}$ at which the average heat capacity has fallen by $\Delta C_p/e$ from its liquid-like value $C_{p\mathrm{l}}$, by analogy with the equivalent temperature $T_{1/e}^*$ discussed above but now defined with respect to the average heat capacity obtained on cooling. In this way, it is possible to determine the cooling rate q_{av} and the modulation period t_{p} such that they define the same transition temperatures, $T_{1/e}^{\mathrm{av}}$ and $T_{1/e}^*$, respectively, thus obtaining a kind of correspondence between the cooling rate and the period (or frequency).

Before proceeding to develop this correspondence, however, it is necessary to note some experimental/computational problems. For a given cooling rate, increasing the modulation period leads to a greater change in temperature and C_p^* during any one period, and to a reduction in the number of periods within the transition interval. For this reason, it is necessary to use a cooling rate sufficiently slow to accommodate the longest period, with the experimental problem that this involves long experimental times and the computational problem that, for the shorter periods, long computational times are involved since it is always necessary to include a minimum number (say 12) of points per cycle for the Fourier transformation procedure, and hence short periods will involve a large number of computation steps. These effects are illustrated in Fig. 6a–c, where the average heat capacity, complex heat capacity and phase angle, respectively, are shown for cooling with $q_{\mathrm{av}} = -0.3\ \mathrm{K\ min^{-1}}$ and with periods between 30 and 300 s.

As expected, the average heat capacity (Fig. 6a) is unaffected by the change of modulation period, apart from the ripples which appear principally at the start of the sigmoidal change, and which are dominated by those at the highest frequency. Thus, as for conventional DSC, the average heat capacity depends only on the underlying cooling rate, which is constant for this series of simulations. On the other hand, the complex heat capacity (Fig. 6b) is shifted to higher temperatures as the frequency increases (period decreases). Besides this shift, however, the quality of the curve rapidly deteriorates as the period increases because of the significant structural changes that occur during such cycles. A close examination of Fig. 6b also reveals a lack of superposability in the lower temperature region of each curve, analogous to the shape changes observed in Fig. 2. These effects are reflected also in the phase angle (Fig. 6c), which becomes more noisy as the period increases, as well as shifting on the temperature scale similar to the shift of C_p^* and reducing in the magnitude of the negative peak height.

From the shift of C_p^* with period it is possible to evaluate the reduced apparent activation energy. Fig. 7 shows these shifts evaluated for both $T_{1/e}^*$ and T_{mid}^*, as well as the equivalent temperatures from the average heat capacity curves (Fig. 6a), $T_{1/e}^{\mathrm{av}}$ and $T_{\mathrm{mid}}^{\mathrm{av}}$. First, it can be seen that the average heat capacity curves are unaffected by the period, as mentioned above. Second, it can be seen that the shift of T_{mid}^* is slightly greater than that of $T_{1/e}^*$, with slopes giving $\Delta h^*/R$ as 73 and 80 kK, respectively. Thus, as before, the shift of the C_p^* curves at the point where the value of C_p^* is reduced by $\Delta C_p/e$ from $C_{p\mathrm{l}}$ recovers the input value of activation energy, whereas a certain error is incurred by the use of the mid-point.

3.4. Effect of underlying cooling rate q_{av}

Analogous to the observed independence of $C_{p,\mathrm{ave}}$ on the modulation period, the complex heat capacity is essentially independent of the underlying cooling rate for a given period. The range of q_{av} is limited, however, as was the range of periods discussed above, by the need to retain sufficient cycles within the transition interval, and by the need to limit the amount

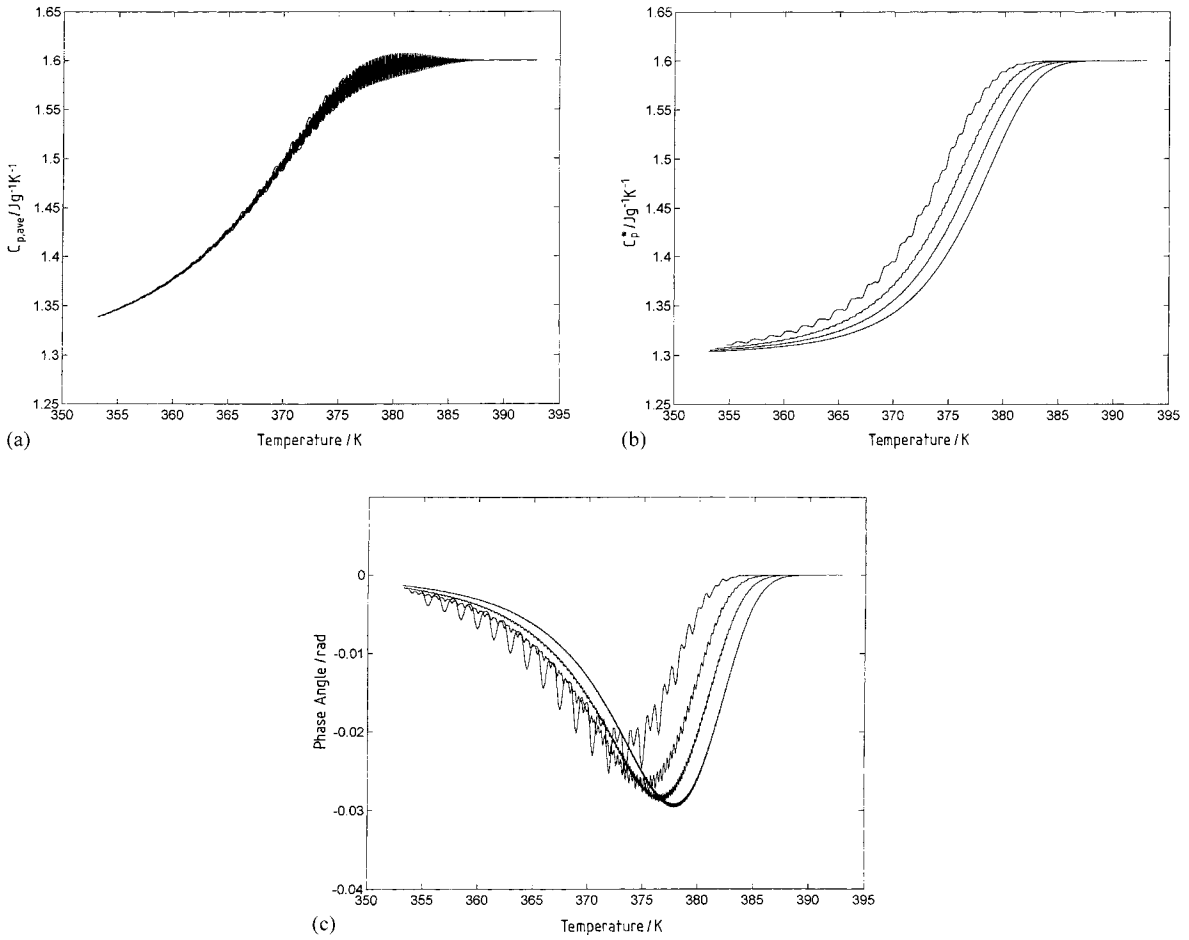

Fig. 6. Average heat capacity (a), complex heat capacity (b), and phase angle (c) during cooling from equilibrium at 393 K with $q_{av} = -0.3$ K min^{-1} and modulation periods of 30, 60, 120 and 300 s, as indicated. Other parameters are: $A_T = 0.5$ K, $\beta = 0.4$ and $x = 0.4$.

of structural change that occurs during any one period. Fig. 8 shows this independence of C_p^* on q_{av}, as well as the dependence of $C_{p,ave}$, for a range of q_{av} of 1 decade and for a modulation period of 30 s. It can be seen that all the curves for $C_{p,ave}$ are displaced as the cooling rate is changed (Fig. 8a), whereas they all approximately superpose for C_p^* (Fig. 8b), if the effect of the ripples is ignored. The phase angle shows the same independence on modulation period as does C_p^*.

An additional feature is also shown in Fig. 8, for the faster cooling rate, i.e. for the curves with the fewest modulations. Although the period was kept constant at 30 s, the analysis was done first with only 12 points per cycle, and was then repeated with 30 points per cycle by using a time step 2.5 times shorter. The effect is hardly noticeable in Fig. 8a for the average heat capacity, but is more so for the complex heat capacity, and even more so for the phase angle, though this is not shown here. The effect is a small displacement of the C_p^* trace to higher values in the transition interval, and a displacement of the phase angle to slightly smaller negative values as the number of points per cycle decreases. This serves to emphasise the need to maintain a sufficient number of points per cycle, though this does not affect the conclusions that we draw from the present analysis. It also shows that the ripples are indeed an artefact of the windowing process that is used for the Fourier transformation.

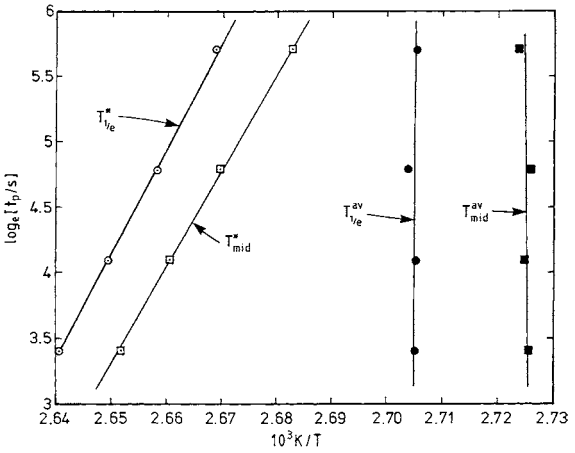

Fig. 7. Plot of log (period) versus reciprocal temperature for the various characteristic temperatures: $T^*_{1/e}$, open circles; T^*_{mid}, open squares; $T^{\mathrm{av}}_{1/e}$, filled circles; $T^{\mathrm{av}}_{\mathrm{mid}}$, filled squares. Data obtained from curves in Fig. 6a and b.

3.5. Effect of period of modulation during cooling when $t_p q_{av}$ = constant

From the foregoing discussion we may draw the following conclusions as regards obtaining the correspondence between cooling rate and frequency of modulation: (i) since the average heat capacity is essentially the same as C_p obtained by conventional DSC, the dependence on cooling rate is best obtained from the latter because it does not involve any ripples; (ii) since the complex heat capacity is independent of the cooling rate, the cooling rate should be changed with the changing period such that sufficient modulations are included in the transition and a reasonable experimental timescale is involved (here we take $q_{\mathrm{av}}t_{\mathrm{p}} = -0.6$ K, as was done for Fig. 2); and (iii) the transition temperatures for both C_p and C^*_p should be evaluated at the point at which C_p or C^*_p has fallen by an amount C_p/e from the equilibrium liquid-like value.

Under these circumstances, the dependence of C^*_p on t_{p} can easily be obtained by simulation, and is shown together with that of the phase angle in Fig. 9a and b, respectively. Here we can immediately see, particularly with respect to the phase angle in Fig. 9b, that the curves are entirely superposable by a shift along the temperature scale, and it is a simple matter to show that one recovers the input reduced activation energy of 80 kK from this shift, making use of either $T^*_{1/e}$ or T^*_{mid}. Not only do these results indicate that the best method for the evaluation of the activation energy using TMDSC experiments is from the dependence of either $T^*_{1/e}$ or T^*_{mid} in the C^*_p curves on cooling at an underlying rate such that $t_{\mathrm{p}}q_{\mathrm{av}}$ is constant, but also this gives a clue as to why the activation energies found from the shifts of $T^*_{1/e}$ or T^*_{mid} are slightly different (cf. Fig. 7) if the condition $t_{\mathrm{p}}q_{\mathrm{av}}$ = constant is not maintained.

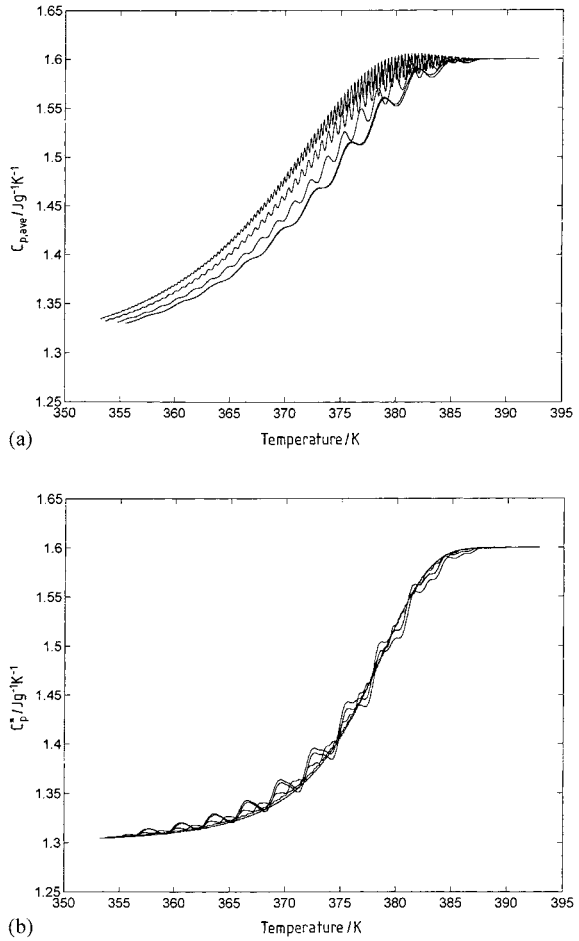

Fig. 8. Average heat capacity (a) and complex heat capacity (b) during cooling at rates −0.6, −1.2, −3 and −6 K min^{-1} from equilibrium at 393 K, with a modulation period of 30 s. Other parameters are: $A_T = 0.5$ K, $\beta = 0.4$ and $x = 0.4$. The two curves in both (a) and (b) with the same number of modulations were obtained using a computation with a different number of points per cycle (see text).

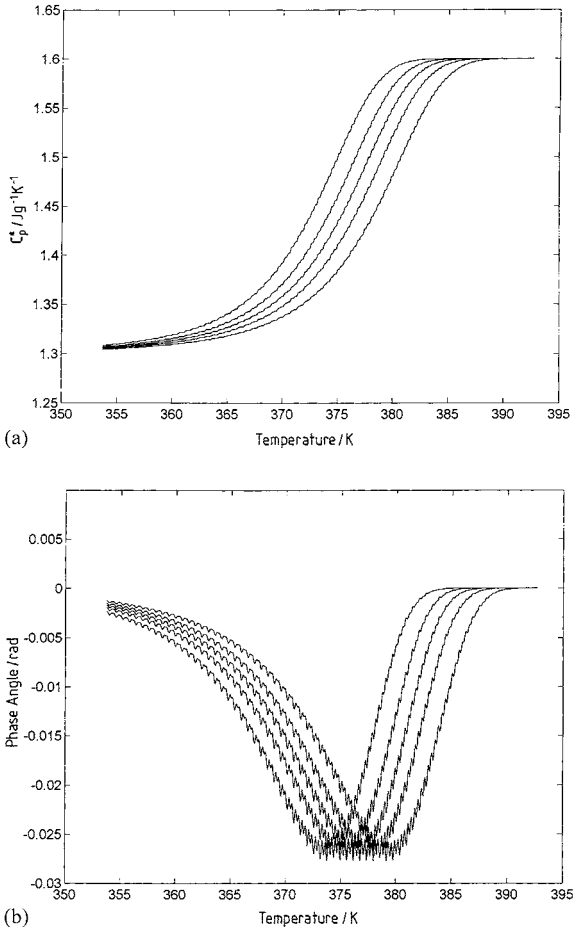

Fig. 9. Family of complex heat capacity (a) and phase angle (b) curves for cooling at rates q_{av} given by $t_p q_{av} = -0.6$ K min^{-1} from equilibrium at 393 K, and for periods $t_p = 12$, 30, 60, 120 and 300 s. Other parameters are: $A_T = 0.5$ K, $\beta = 0.4$ and $x = 0.4$.

The reason is that the liquid-to-glass transition is occurring simultaneously by two paths, both of them controlled by the underlying cooling rate but measured on different timescales: the average heat capacity gives the "conventional" (or called "thermal" by some authors [17]) glass transition at a temperature determined by the timescale of the underlying cooling rate, while the complex heat capacity gives a "dynamic" glass transition at a temperature determined by the timescale of the modulations. What is important in the present context is that these timescales overlap for typical experimental values of q_{av} and t_p, which means that the dynamic glass transition observed experimentally will not, in general, occur independently of the conventional glass transformation process. This can be seen, in fact, by comparing the temperature ranges over which the transition occurs in $C_{p,ave}$ and C_p^* in Fig. 6a and b, or in Fig. 8a and b. It is clear in both cases that, for the ranges of underlying cooling rates and modulation frequencies selected here, the major part of the transition in C_p^* occurs simultaneously with that in $C_{p,ave}$. In order to avoid this overlap of the two transitions, it would be necessary either to increase the modulation frequency and/or reduce the underlying heating rate. This will usually not be wholly possible, as it would involve either experimentally inaccessible frequencies or inordinately slow cooling rates. Similar ideas to these have been presented by Weyer and Schick [35].

3.6. Correspondence between cooling rate q_{av} and period t_p

In the light of the above considerations, we can compare the timescales for $C_{p,ave}$ and C_p^* by determining the corresponding underlying cooling rate and frequency (or period), respectively, that will give equal values for their respective transition temperatures, $T_{1/e}^{av}$ and $T_{1/e}^*$. In fact this is more conveniently done for $T_{g,1/e}$, the equivalent to $T_{1/e}^{av}$ but obtained from a conventional DSC cooling curve, and $T_{1/e}^*$. For example, Fig. 10 shows the cooling curves for conventional

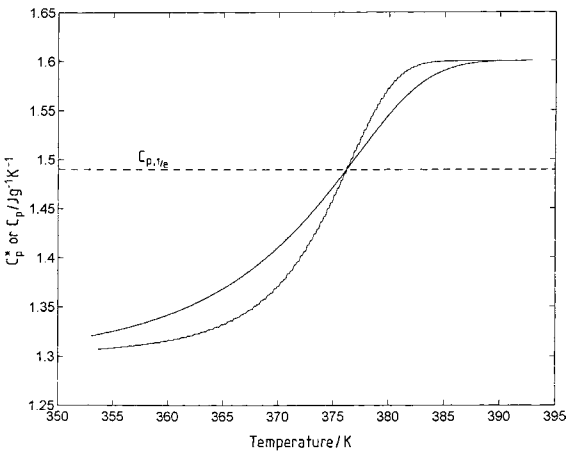

Fig. 10. Cooling curves for conventional DSC, with cooling rate of -13.06 K min^{-1}, and C_p^* from TMDSC with $q_{av} = -0.3$ K min^{-1} and $t_p = 120$ s. Other parameters are as follows: $\Delta h^*/R = 80$ kK, $A_T = 0.5$ K, $\beta = 0.4$, and $x = 0.4$.

DSC, at a rate of $q = -13.06\ \mathrm{K\ min^{-1}}$, and for C_p^* from TMDSC with $q_{\mathrm{av}} = -0.3\ \mathrm{K\ min^{-1}}$ and a period of 120 s. The latter is clearly sharper and displays ripples, and the two curves cross at a value of C_p or C_p^* that is $\Delta C_p/e$ less than $C_{p\mathrm{l}}$. It is convenient to compare the conventional DSC cooling rate q and the TMDSC period t_{p} in terms of a logarithmic difference, Δ, defined by

$$\Delta = \Delta(\mathrm{e}, \mathrm{Ks^{-1}}, \mathrm{s}) = \log_e[|q|] + \log_e[t_{\mathrm{p}}] \tag{16}$$

where $|q|$ is in $\mathrm{K\ s^{-1}}$ and t_{p} in seconds. Clearly this difference in general depends on the choice of units for each of q and t_{p}, and on whether natural or decimal logarithms are used; in addition one can define the difference with respect to the angular frequency of modulation ω rather than the period t_{p}. An alternative definition of the logarithmic difference which has been used by Schick and co-workers [36–38] is

$$\begin{aligned}\Delta(10, \mathrm{Ks^{-1}}, \mathrm{rad\ s}) &= \log_{10}[|q|] - \log_{10}[\omega] \\ &= \frac{\Delta}{2.303} - 0.798\end{aligned} \tag{17}$$

where $|q|$ is in $\mathrm{K\ s^{-1}}$ and ω in $\mathrm{rad\ s^{-1}}$. Here we make use of the definition of Δ in Eq. (16), but note that other differences may be related simply to Δ, for example by Eq. (17). In the present case, for the results shown in Fig. 10, for which $\beta = 0.4$ and $x = 0.4$, we find $\Delta = 3.263$, very close to the value of $\Delta = 3.25$ obtained for $x = 0.4$ with the earlier single relaxation time model (see Table 1 in [11]). The same procedure can be used to determine Δ for any combination of values of β and x, and the full set of results is presented in Table 1.

It has been argued, principally by Schick and co-workers [36–38], and based upon the fluctuation dissipation theorem for the glass transition [39–41], that the angular frequency of modulation, ω ($\mathrm{rad\ s^{-1}}$) in TMDSC and the cooling rate $|q|$ ($\mathrm{K\ s^{-1}}$) in conventional DSC can be related by an equation:

$$\omega = \frac{|q|}{a\,\delta T} \tag{18}$$

where a is a constant and δT is the mean temperature fluctuation of the cooperatively rearranging regions. It has commonly been found by these workers that a is of the order of 6 ± 2 and $\delta T \approx 2.5$ K, giving $a\,\delta T \approx 15 \pm 5$ K. We can likewise evaluate $a\,\delta T$ from the results in Table 1 by writing

$$a\,\delta T = \frac{|q|}{\omega} = \frac{|q| t_{\mathrm{p}}}{2\pi} \tag{19}$$

which, since $t_{\mathrm{p}} = 120$ s in these simulations, gives $a\,\delta T = |q|/\pi$, when $|q|$ has units of $\mathrm{K\ min^{-1}}$. The resulting values of $a\,\delta T$ are included in Table 1. A number of observations can be made from these tabulated results.

First, we note that, for any given value of x, as β decreases from unity, i.e. as the distribution of relaxation times broadens, the cooling rate required to achieve the same transition temperature as that found from TMDSC increases, and hence the logarithmic difference Δ also increases. This effect can be understood quite simply. As β decreases, the response broadens, and this can be seen clearly in the $C_{p,\mathrm{ave}}$ curves. Hence, whatever temperature is used (e.g. T_{mid} or $T_{1/e}$) to define a transition temperature, it will decrease relative to the onset of the transition as the distribution broadens. Therefore, in order to maintain the DSC transition temperature at the same value as that from TMDSC, it is necessary continuously to increase the cooling rate for DSC in order to compensate for this broadening effect.

The range of cooling rates that emerges from these simulations, for a typical experimental modulation period of 120 s, is from about -5 to about -25 K $\mathrm{min^{-1}}$, which is a typical range that might be used in conventional DSC. The underlying cooling rate in the TMDSC simulations was $-0.3\ \mathrm{K\ min^{-1}}$, and hence between 1 and 2 decades slower than the DSC range. With the reduced apparent activation energy of 80 kK, again typical of experimental values for polymers, this difference in rates is equivalent to a shift of between about 4 and 8 K (for example, refer to Fig. 8a). Since the DSC rates in Table 1 give the same transition temperature as for TMDSC with $t_{\mathrm{p}} = 120$ s, the implication is that the average heat capacity curve from TMDSC will be shifted by only approximately 4–8 K from the complex heat capacity curve, the shift depending on the values of β and x. Thus, as we observed earlier, there will inevitably be an interaction between the underlying response and the dynamic response since the transition interval will surely be significantly greater than these shifts of 4–8 K, typical values being 15 K or more.

Table 1
Correspondence between cooling rate q in conventional DSC and period $t_p = 120$ s in TMDSC (with $q_{av} = -0.3$ K min^{-1}) to give the same transition temperature $T_{1/e}$, for full ranges of values of β and x[a]

β	x	$T_{1/e}$ (K)	$\lvert q \rvert$ (K min^{-1})	Δ	$a\,\delta T$ (K)
0.2	0.2	375.73	24.51	3.892	7.80
	0.3	375.86	20.68	3.722	6.58
	0.4	375.92	16.98	3.525	5.40
	0.6	376.16	12.88	3.249	4.10
	1.0	376.50	7.72	2.737	2.46
0.3	0.2	376.10	21.00	3.738	6.68
	0.3	376.14	17.72	3.568	5.64
	0.4	376.16	14.97	3.399	4.77
	0.6	376.21	11.13	3.103	3.54
	1.0	376.48	7.46	2.703	2.37
0.4	0.2	376.14	17.85	3.575	5.68
	0.3	376.16	15.19	3.414	4.84
	0.4	376.18	13.06	3.263	4.16
	0.6	376.22	10.11	3.007	3.22
	1.0	376.45	7.13	2.658	2.27
0.6	0.2	376.11	14.41	3.361	4.59
	0.3	376.13	12.60	3.227	4.01
	0.4	376.15	11.09	3.099	3.53
	0.6	376.18	8.79	2.727	2.80
	1.0	376.26	6.05	2.493	1.93
0.8	0.2	375.92	11.62	3.146	3.70
	0.3	375.93	10.17	3.013	3.24
	0.4	375.95	9.03	2.894	2.87
	0.6	376.10	7.78	2.745	2.48
	1.0	376.18	5.50	2.398	1.75
1.0	0.2	375.85	10.39	3.034	3.31
	0.3	375.87	9.18	2.910	2.92
	0.4	375.88	8.15	2.791	2.59
	0.6	375.90	6.57	2.576	2.09
	1.0	375.98	4.70	2.241	1.50

[a] The logarithmic difference Δ is defined by Eq. (16), and $a\,\delta T$ is evaluated from Eq. (19).

The effect of x is similar to that of β in that the logarithmic difference Δ decreases as the relaxation process becomes sharper, either through β or x tending towards unity. The overall range of values of Δ is from 2.24 to 3.89, encompassing typical values that are observed experimentally in our laboratories [42,43]. For example, Jiang [42] finds logarithmic differences of $\Delta = 3.4 \pm 0.2$ for polystyrene and 3.2 ± 0.2 for polycarbonate, while Montserrat [43] obtains $\Delta = 2.9 \pm 0.2$ for a fully cured and stoichiometric epoxy-amine resin. This range of values is also very similar to that found earlier for the single relaxation time model simulations [11], which was from 2.40 to 3.70 for the same values of x as used here, from 0.2 to 1.0.

However, these differences Δ listed in Table 1, and the corresponding values of $a\,\delta T$, are significantly different from those found by Schick and co-workers [36–38] and Donth and co-workers [41]. These authors report logarithmic differences Δ in the range 4.37–5.98 for a variety of glass forming systems, both polymeric and inorganic. One possible reason for this is that these authors compare frequency and cooling rate at the mid-point transition temperature which, for the reason discussed above, would lead to larger values of Δ than those evaluated for $T_{1/e}$. The present

Table 2
Correspondence between cooling rate q in conventional DSC and period $t_p = 120$ s in TMDSC (with $q_{av} = -0.3$ K min^{-1}) to give the same transition temperature T_{mid}, for selected values of β and x[a]

β	x	T_{mid} (K)	$\lvert q \rvert$ (K min^{-1})	Δ	$a\,\delta T$ (K)
0.2	0.2	371.95	68.79	4.924	21.9
	0.4	372.30	33.24	4.197	10.6
	1.0	373.32	8.54	2.838	2.72
0.4	0.2	374.40	43.94	4.476	14.0
	0.4	374.57	26.14	3.957	8.32
	1.0	374.94	8.98	2.888	2.86
1.0	0.2	375.27	25.72	3.940	8.19
	0.4	375.31	16.43	3.492	5.23
	1.0	375.55	7.27	2.677	2.31

[a] The logarithmic difference Δ is defined by Eq. (16), and $a\,\delta T$ is evaluated from Eq. (19).

model has, therefore, also been used to compare cooling rate and frequency for the same value of T_{mid}, and the results are presented in Table 2.

It can be seen that, as expected, the values of Δ are increased over the whole range, now increasing from 2.68 to 4.92 as both β and x decrease. However, the majority of values of Δ remain smaller than those found by Schick and co-workers and Donth and co-workers, and in fact there are still several values of these authors that are greater than any values in Table 2. It is, therefore, difficult to reconcile the present model with these authors' results, though it is well known that the TNM equation suffers from some inadequacies, and hence that some of the basic assumptions of this model, such as the use of a constant apparent activation energy, may need to be re-assessed. On the other hand, there is also a certain discrepancy in the trend of Δ as well as in its absolute value. In the present model, the results in Tables 1 and 2 show that the logarithmic difference Δ increases as β and/or x decrease, which usually relates to an increase in the fragility of the glass-former. Thus, one might anticipate the inorganic glass DGG and the sodium-silicate glass in Hensel and Schick's work [38], which are strong glass-formers with an approximately Arrhenius temperature dependence, to have relatively small values of Δ, while the polymers, which are generally fragile glass-formers, would be expected to have higher values of Δ. The main trend of the results of Hensel and Schick [38] is the opposite, however. There is clearly a need for a further examination of the relationship between the conventional and dynamic glass transitions.

3.7. Comparison of conventional and dynamic glass transitions

At this point it is perhaps worth considering why the transitions in C_p on cooling are so different in respect of the average and complex heat capacities; in the former the transition (conventional) is much broader than in the latter (dynamic). As discussed earlier, the timescales are quite different for the two transitions, but this in itself does not explain the observation. The real explanation lies in whether or not the measurements are made in equilibrium. For the average heat capacity, the state of the sample begins to depart from equilibrium as the transition begins on cooling, which has the effect of reducing the rate at which the relaxation time increases. This effect occurs by virtue of the non-linearity of the system, and is determined by the parameter x, being a stronger effect the smaller is x, or the greater is the non-linearity (refer to Eq. (3)). This departure from equilibrium, and the associated relative increase of the relaxation time, means that the temperature must be reduced further in order to achieve a relaxation time sufficiently long that the response becomes completely glassy for the rate of cooling imposed. Of course, the continued reduction of temperature drives the system further away from equilibrium, and hence, the transition is spread over a temperature range that is broader the smaller is the value of x.

As an illustration, the relaxation time is plotted, on a logarithmic scale, as a function of reciprocal temperature in Fig. 11, for the choice of $\beta = 1.0$ and $x = 0.4$

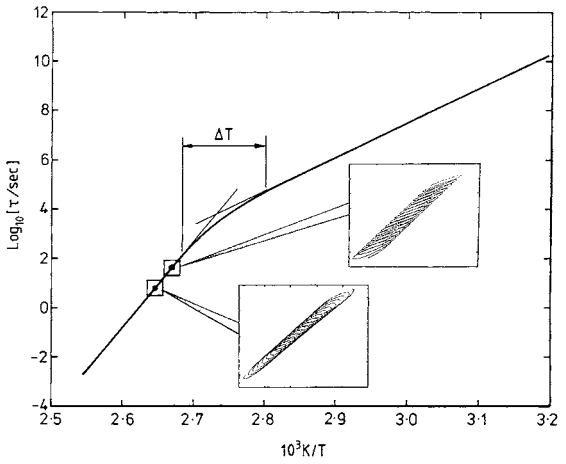

Fig. 11. Theoretical dependence of log (relaxation time) as a function of reciprocal temperature during cooling through glass transition region. Full line shows dependence for conventional DSC with $q = -0.125$ K min^{-1}, and ΔT indicates the temperature range over which C_p decreases from 1.57 to 1.33 J g^{-1} K^{-1}, a decrease of 80% of ΔC_p centred on its midpoint value. The points represent the values of τ and $1/T$ at which C_p^* in TMDSC experiments, with $q_{av} = -0.125$ K min^{-1}, likewise takes values of 1.57 and 1.33 J g^{-1} K^{-1}, while the insets are expanded views of the regions around these points. The parameters are $\beta = 1.0$, $x = 0.4$ and $\Delta h^*/R = 80$ kK, and for the TMDSC simulation $t_p = 60$ s and $A_T = 0.5$ K.

and for a cooling rate of -0.125 K min^{-1}. The conventional glass transition temperature is found as the intersection of the extrapolated liquid and glassy lines, as shown. The breadth of the transition is measured here (arbitrarily) by ΔT, the temperature interval over which C_p falls from 10% of ΔC_p less than C_{pl} (1.57 J g^{-1} K^{-1}) to 10% of ΔC_p more than C_{pg} (1.33 J g^{-1} K^{-1}).

For the complex heat capacity, on the other hand, the time scale is (generally) shorter than that equivalent to the underlying cooling rate, so that the transition occurs at a higher temperature. If this transition temperature is sufficiently far above that which corresponds to the cooling rate (i.e. if the period is sufficiently short or the underlying cooling rate is sufficiently slow), then the transition will occur when the relaxation time, in equilibrium, becomes longer than the modulation period. There is no non-linear broadening of the transition as there is for the cooling rate transition, since the system is continuously in quasi-equilibrium until the transition is reached. It is, therefore, just the temperature dependence of the relaxation time in equilibrium which determines when this dynamic transition will occur. In Fig. 11, the start ($C_p^* = 1.57$ J g^{-1} K^{-1}) and finish ($C_p^* = 1.33$ J g^{-1} K^{-1}) of the dynamic transition are shown as dots on the high temperature, equilibrium, portion of the conventional DSC curve for logarithmic relaxation time. The insets show, for the temperature interval indicated by each box, the cyclic dependence of log τ as a function of reciprocal temperature. It is clear that the higher temperature box shows a dynamic response that is liquid-like and closely follows the equilibrium line, whereas the lower temperature box shows a dynamic response that is glassy but still moves along the equilibrium line. The temperature interval between the dynamic liquid-like and dynamic glassy response is clearly significantly less than ΔT for the conventional DSC, or average C_p response.

Of course, this argument must be modified slightly for the situation in which the dynamic glass transition overlaps some part of the underlying glass transition. Under these circumstances, the departure of the system from equilibrium implies a relative increase in the relaxation time, and hence a broadening of the dynamic glass transition in just the same way as discussed above for the average heat capacity. In fact, for reasons considered earlier and evident from the correspondence between cooling rate and modulation period, the usual experimental condition is such that the two transitions do indeed overlap. In this case, the dynamic transition will not represent simply the equilibrium frequency response of the heat capacity, and care should, therefore, be exercised in the interpretation of the complex heat capacity or phase angle curves. This broadening effect due to the overlap of the two transitions may contribute to the large values of Δ observed by Hensel and Schick [38], and may also be the reason why activation energies measured by TMDSC are often much smaller than those measured by conventional DSC techniques.

3.8. Effects of non-linearity parameter x and non-exponentiality parameter β

The smaller is the non-linearity parameter x, the greater is the contribution of structure, either defined by the excess enthalpy δ (Eq. (2)) or by the fictive temperature T_f (Eq. (3)), to the relaxation time, and

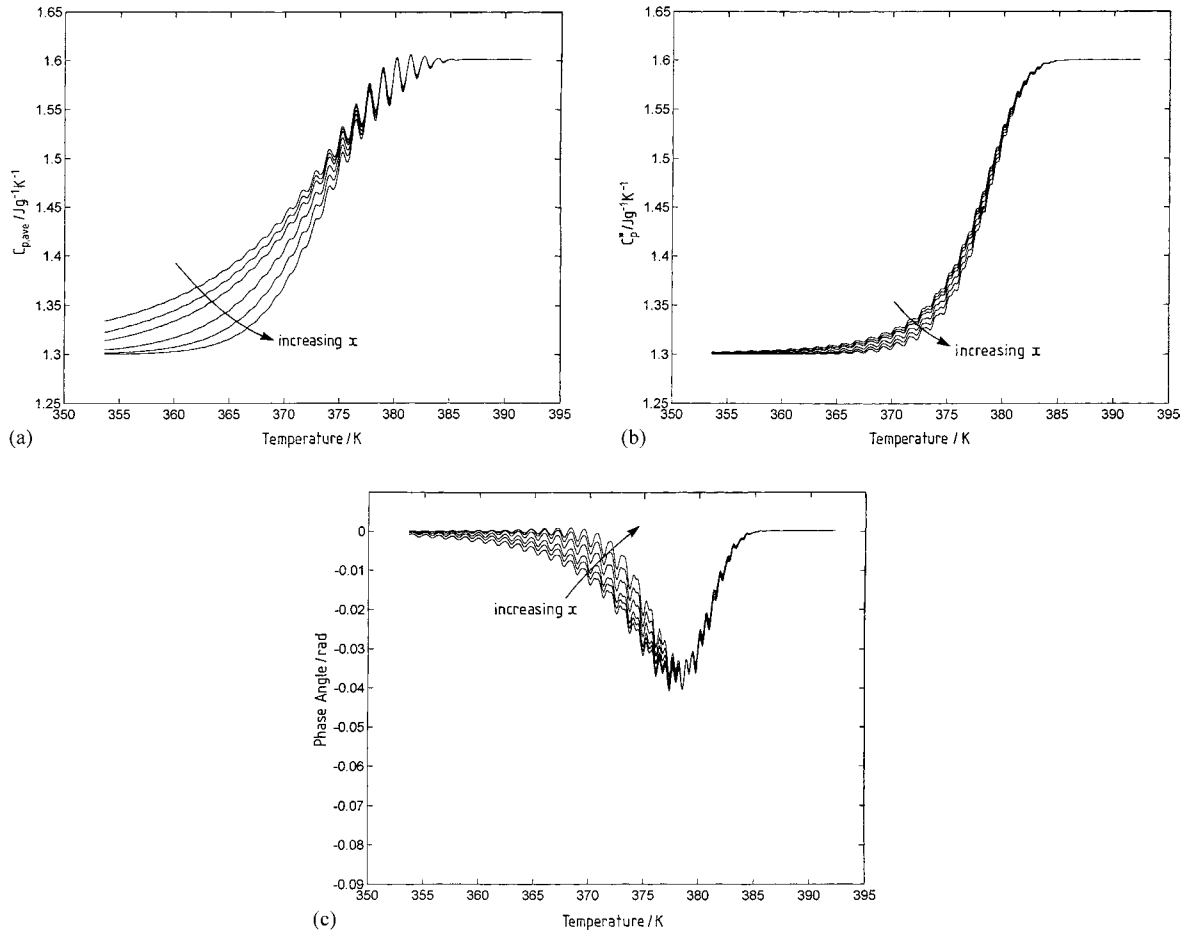

Fig. 12. Cooling curves for TMDSC with $q_{av} = -3$ K min^{-1}, $t_p = 24$ s, $A_T = 0.5$. K, $\beta = 0.6$ and $x = 0.2, 0.3, 0.4, 0.6, 0.8$ and 1.0. (a) $C_{p,ave}$; (b) C_p^*; and (c) ϕ.

hence the glass transition observed in conventional DSC will occur at lower temperature the smaller is the value of x. At the same time, the increased non-linearity means that the transition is broadened, and the overall effect is as illustrated by the average heat capacity curves shown for a range of values of x in Fig. 12a.

In contrast, this significant broadening as x decreases is not evident in either the complex heat capacity (Fig. 12b) or the phase angle (Fig. 12c). Here we see instead only a rather small effect when x is varied over essentially its full range. This, as will be seen shortly, has an important implication in respect of the experimental evaluation of the non-exponentiality parameter β.

Turning now to the effect of β, shown in Fig. 13, we see that the effect on the average heat capacity, seen in Fig. 13a, is very similar to that of the non-linearity parameter, involving a broadening of the transition as the value of β decreases. This is to be anticipated intuitively, since one would expect a broader response from a wider distribution of relaxation times. Whereas the dependence on x is seen in Fig. 12a as a fanning out of the curves from a unique value of C_{pl} at a temperature of approximately 385 K, however, the dependence on β in Fig. 13a displays a cross-over of all the curves at a unique value of $C_{p,ave}$; this value is $\Delta C_p/e$ less than C_{pl}, and again emphasises the importance of this point, as mentioned earlier. Defining the glass transition temperature with respect to this point,

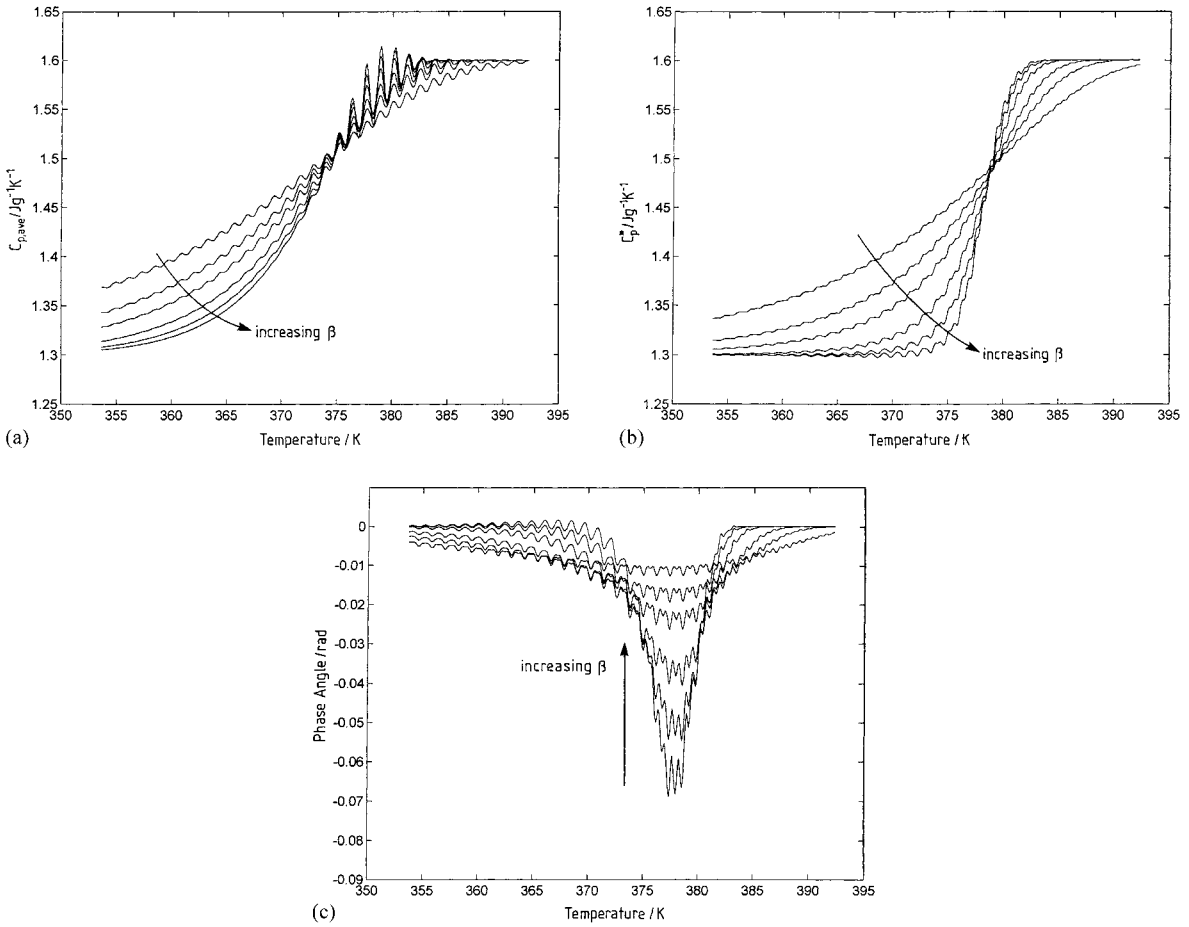

Fig. 13. Cooling curves for TMDSC with $q_{av} = -3$ K min^{-1}, $t_p = 24$ s, $A_T = 0.5$ K, $x = 0.4$ and $\beta = 0.2$, 0.3, 0.4, 0.6, 0.8 and 1.0. (a) $C_{p,ave}$; (b) C_p^*; and (c) ϕ.

namely as $T_{g,1/e}$, therefore, implies no dependence of the transition temperature on β, with reducing β simply broadening the transition in the temperature range above and below $T_{g,1/e}$. On the other hand, defining the glass transition temperature with respect to the mid-point temperature, namely as $T_{g,mid}$, would imply a reduction in the transition temperature as β decreased, i.e. as the distribution of relaxation times broadened.

Whereas the effects of x and β on the average heat capacity are somewhat similar, however, their effect on C_p^* and the phase angle are fundamentally different. Both C_p^* and ϕ were shown to be essentially independent of x in Fig. 12b and c, but it can be seen from Fig. 13b and c that this is certainly not the case in respect of the effect of β; varying β between 0.2 and 1.0 leads to a dramatic sharpening of the transition in C_p^* and an approximately seven-fold reduction in the maximum negative phase angle.

This has an important implication, since it means that C_p^* and ϕ are experimentally measurable parameters that are essentially independent of x but sensitive to β, thus affording a possible procedure for the independent evaluation of β from experimental data. The determination of β has in the past usually been made either by curve-fitting (e.g. see [44]), in which heat capacity data are fitted by simultaneously adjusting several parameters, including x and β, or by examining the height of the endothermic peak, on heating, as a function of the prior cooling rate [34],

Table 3
Values of $\overline{S}$ (Eq. (20)) from Fig. 13b and of $\overline{S}/\theta$ where $\theta = \Delta h^*/RT_g^2$ as a function of β

β	$\overline{S}$ (K^{-1})	$\overline{S}/\theta$
0.2	0.0363	0.063
0.3	0.0553	0.096
0.4	0.0743	0.129
0.6	0.1150	0.200
0.8	0.1550	0.270
1.0	0.2023	0.352

when the value of x is already known from the peak-shift method [26,27]. Since the phase angle ϕ is subject to substantial ripples, and furthermore appears to have a more complicated dependence than does C_p^*, the procedure suggested here would be to evaluate the inflectional slope of C_p^* as a function of temperature, normalised with respect to ΔC_p:

$$\overline{S} = \frac{1}{\Delta C_p}\frac{dC_p^*}{dT} \tag{20}$$

This quantity has been found from Fig. 13b and is given in Table 3 as a function of β. It can be seen that $\overline{S}$ is very sensitive to the values of β. However, it transpires also that $\overline{S}$ depends linearly on the apparent activation energy, implying that it should be normalised also with respect to this. A similar correlation was found by Moynihan [45], who observed a constancy of $\Delta h^*(1/T_g - 1/T_g')$, where T_g and T_g' mark the beginning and end, respectively, of the transition region. Writing this as a constancy of $\Delta h^* \Delta T/\Delta T_g^2$, where ΔT is the width of the transition region, it can easily be seen that this implies $\theta\,\Delta T$ is constant, equivalent to a linear dependence of $\overline{S}$ on θ, where θ is the KAHR equivalent of the apparent activation energy (see Eq. (2)). Hence an appropriate way of normalising $\overline{S}$ is to consider the dimensionless quantity $\overline{S}/\theta$, which would be a suitable quantity for the evaluation of β, and which has been included in Table 3. The suggested procedure would, therefore, be to evaluate the normalised and dimensionless inflectional slope $\overline{S}/\theta$ experimentally by TMDSC, for any given polymer during cooling through the glass transition interval, and then to compare this with the values given in Table 3 in order to determine β.

As an illustration, we have evaluated $\overline{S}$ for polycarbonate using Mettler–Toledo's ADSC with cooling

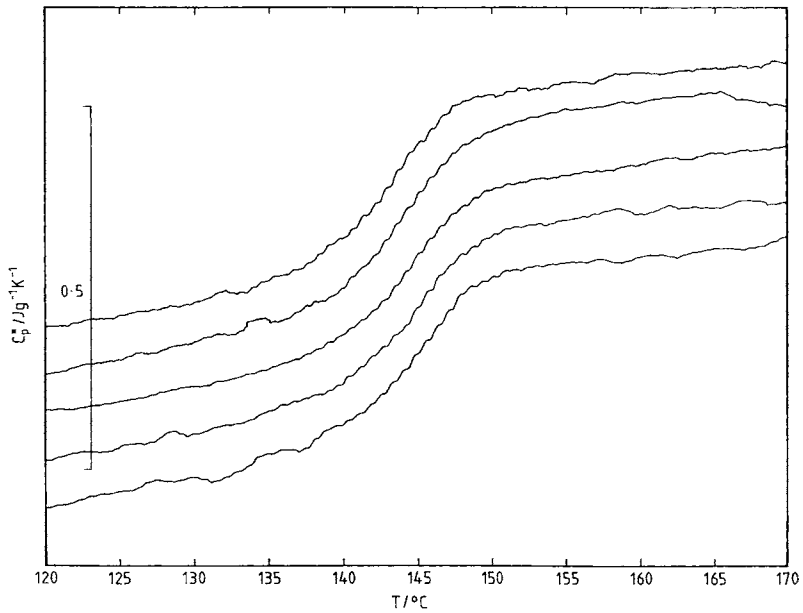

Fig. 14. Experimental complex heat capacity obtained by ADSC from cooling curves using polycarbonate, over the temperature range from 175 to 115°C. Cooling rates are 0.5, 1.0, 1.5, 2.0, and 3.0 K min^{-1} with an amplitude $A_T = 0.5$ K and period adjusted such that $t_p|q_{av}| = 1.5$ K. Note that the heat capacity scale is relative, and that curves are shifted vertically for clarity.

rates $|q_{av}|$ in the range from 0.5 to 3.0 K min^{-1} and period t_p such that $t_p|q_{av}| = 1.5$ K. The amplitude of temperature modulations was 0.5 K, and the curves of complex heat capacity as a function of temperature are shown in Fig. 14. The inflectional tangent from these curve gives $\overline{S} \approx 0.11$ K^{-1}, essentially independent of the underlying cooling rate. For this same polycarbonate we previously determined $\Delta h^*/R = 140$ kK [46], which for $T_g = 418$ K gives $\theta = 0.80$ K^{-1}. Hence from the value of $\overline{S}/\theta = 0.14$ we find from Table 3 a value of β for polycarbonate slightly greater than 0.4. This is in satisfactory agreement with the value obtained for the same polycarbonate using enthalpy relaxation analysis [46], which estimated β to lie within the range $0.456 < \beta < 0.6$.

Finally, in respect of the simulation curves shown in Fig. 13a and b for the effect of β, it can be seen once again that all the curves for $C_{p,ave}$ and C_p^* pass through a unique point at a value of heat capacity which is $\Delta C_p/e$ less than the liquid-like value, C_{pl}. This once more reinforces our suggestion that this is the important point on the complex or average heat capacity curves which should be used for the quantitative analysis of the data.

4. Conclusions

An analysis of TMDSC in the glass transition region has been presented, in which a distribution of relaxation times has been incorporated into an earlier single relaxation time model. The parameters of the present analysis are the non-exponentially parameter β of the KWW distribution function, the non-linearity parameter x, and the apparent activation energy Δh^*. It is shown that the model describes, more realistically than its predecessor, all of the characteristic features of TMDSC in the glass transition region.

The effect of the period of modulation during heating and/or cooling through the transition region and the effect of the underlying cooling rate have been studied, and it is shown that some distortion of the complex heat capacity trace can result from an interaction with the underlying glass transformation process during cooling. In particular, under typical experimental conditions this is likely to be the case for polymeric systems, and for a quantitative interpretation of the data it is recommended that experiments be conducted such that the product of period and underlying cooling rate remains constant.

A comparison of conventional DSC and TMDSC responses has been used to identify the correspondence between cooling rate in the former and period in the latter such that the same transition temperature is obtained. For this comparison, it is recommended that the temperature $T_{1/e}$, at which the heat capacity, in either conventional or TMDSC experiments, is reduced by $\Delta C_p/e$ from its liquid-like value, to give a value of $C_{p,1/e}$, should be used as the measure of the transition temperature. This correspondence is used to identify the mean temperature fluctuations of Donth's fluctuation dissipation theorem as a function of the parameters β and x. It is found that the magnitude of the fluctuation increases the wider is the distribution of relaxation times (small β) and the greater is the non-linearity of the relaxation kinetics (small x).

Finally, the effects of the parameters β and x are examined in respect of the average and complex heat capacities on cooling. For $C_{p,ave}$, both β and x have the effect of broadening the transition as they are reduced in value, with all curves for different β passing through a unique point at $C^*_{p,1/e}$. In contrast, for C_p^* the effect of reducing x is insignificant in comparison with that of reducing β, which greatly broadens the transition and increases the magnitude of the maximum phase angle. Thus the breadth of the transition in C_p^* is identified as a measure of β which is essentially independent of the non-linearity parameter x. In practice, since this breadth depends also on the value of ΔC_p and on the apparent activation energy, or its equivalent θ in the KAHR model, it is suggested that a normalised and dimensionless quantity $\overline{S}/\theta$ be used for the evaluation of β by comparison of experimental and theoretical values, where $\overline{S}$ is the inflectional slope of C_p^* versus T (evaluated at $C^*_{p,1/e}$) normalised by dividing by ΔC_p. Experimental data for polycarbonate are used to illustrate the evaluation of β by this procedure.

Acknowledgements

JMH acknowledges the Royal Society (UK) for a European Science Exchange Programme grant which facilitated the completion of this work. Partial support from the Spanish Ministry of Education and Science,

CICYT Project no. MAT 97-0634-C02-02 is also acknowledged.

References

[1] J.C. Seferis, I.M. Salin, P.S. Gill, M. Reading, Proc. Acad. Greece 67 (1992) 311.
[2] P.S. Gill, S.R. Sauerbrunn, M. Reading, J. Thermal Anal. 40 (1993) 931.
[3] M. Reading, D. Elliot, V.L. Hill, J. Thermal Anal. 40 (1993) 949.
[4] M. Reading, Trends Polym. Sci. 1 (1993) 248.
[5] J.E.K. Schawe, Thermochim. Acta 260 (1995) 1.
[6] J.M. Hutchinson, A.B. Tong, Z. Jiang, Thermochim. Acta 335 (1999) 27.
[7] S. Montserrat, J. Polym. Sci., Polym. Phys. Ed. 38 (2000) 2272.
[8] D.J. Hourston, M. Song, A. Hammiche, H.M. Pollock, M. Reading, Polymer 37 (1996) 243.
[9] J.M. Hutchinson, S. Montserrat, J. Thermal Anal. 47 (1996) 103.
[10] J.M. Hutchinson, S. Montserrat, Thermochim. Acta 286 (1996) 263.
[11] J.M. Hutchinson, S. Montserrat, Thermochim. Acta 305 (1997) 257.
[12] J.M. Hutchinson, C.T. Imrie, Z. Jiang, Mettler Toledo USER COM no. 6, 1997, p. 22.
[13] S. Montserrat, J. Thermal Anal. Cal. 59 (2000) 289.
[14] J.E.K. Schawe, W. Winter, Thermochim. Acta 298 (1997) 9.
[15] B. Schenker, F. Stäger, Thermochim. Acta 304/305 (1997) 219.
[16] I. Hatta, A.A. Minakov, Thermochim. Acta 330 (1999) 39.
[17] S. Weyer, A. Hensel, C. Schick, Thermochim. Acta 304/305 (1997) 267.
[18] Z. Jiang, C.T. Imrie, J.M. Hutchinson, Thermochim. Acta 315 (1998) 1.
[19] Z. Jiang, C.T. Imrie, J.M. Hutchinson, Thermochim. Acta 336 (1999) 27.
[20] C.T. Imrie, Z. Jiang, J.M. Hutchinson, Mettler Toledo USER COM no. 6, 1997, p. 20.
[21] S.L. Simon, G.B. McKenna, Thermochim. Acta 307 (1997) 1.
[22] S.L. Simon, G.B. McKenna, J. Chem. Phys. 107 (1997) 8678.
[23] S.L. Simon, G.B. McKenna, Thermochim. Acta 348 (2000) 77.
[24] C. Schick, in: Proceedings of the 6th Lähnwitz Seminar.
[25] J.E.K. Schawe, in: Proceedings of the 6th Lähnwitz Seminar.
[26] A.J. Kovacs, J.M. Hutchinson, J. Polym. Sci., Polym. Phys. Ed. 17 (1979) 2031.
[27] A.J. Kovacs, J.J. Aklonis, J.M. Hutchinson, A.R. Ramos, J. Polym. Sci., Polym. Phys. Ed. 17 (1979) 1097.
[28] A.Q. Tool, J. Am. Ceram. Soc. 29 (1946) 240.
[29] O.S. Narayanaswamy, J. Am. Ceram. Soc. 54 (1971) 491.
[30] C.T. Moynihan, A.J. Easteal, M.A. DeBolt, J. Tucker, J. Am. Ceram. Soc. 59 (1976) 12.
[31] F. Kohlrausch, Annalen der Physik und Chemie 128 (1866) 1, 207, 399.
[32] G. Williams, D.C. Watts, Trans. Faraday Soc. 66 (1970) 80.
[33] M. Ruddy, J. M Hutchinson, Polym. Commun. 29 (1988) 132.
[34] J.M. Hutchinson, M. Ruddy, J. Polym. Sci., Polym. Phys. Ed. 28 (1990) 2127.
[35] S. Weyer, C. Schick, in: Proceedings of the 6th Lähnwitz Seminar.
[36] A. Hensel, J. Dobbertin, J.E.K. Schawe, A. Boller, C. Schick, J. Thermal Anal. 46 (1996) 935.
[37] S. Weyer, A. Hensel, J. Korus, E. Donth, C. Schick, Thermochim. Acta 304/305 (1997) 251.
[38] A. Hensel, C. Schick, J. Non-Cryst. Solids 235–237 (1998) 510.
[39] E. Donth, Glasübergang, Akademie Verlag, Berlin, 1981.
[40] E. Donth, Relaxation and Thermodynamics in Polymers, Glass Transition, Akademie Verlag, Berlin, 1993.
[41] E. Donth, J. Korus, E. Hempel, M. Beiner, Thermochim. Acta 304/305 (1997) 239.
[42] Z. Jiang, Ph.D. Thesis, University of Aberdeen, UK, 2000.
[43] S. Montserrat, unpublished data.
[44] I.M. Hodge, J. Non-Cryst. Solids 169 (1994) 211.
[45] C.T. Moynihan, J. Am. Ceram. Soc. 76 (1993) 1081.
[46] J.M. Hutchinson, S. Smith, B. Horne, G. Gourlay, Macromolecules 32 (1999) 5046.